ACS Pharmacology & Translational Science

pubs.acs.org/ptsci
Article

Broadly Applicable Bispecific Linker Approach to Noncovalently Target Therapeutic Nanoparticles to Tumor Cells Expressing Carcinoembryonic Antigen

Ann Fernando,[‖] Amanda Sparkes,[‖] Esther I. Matus, Ayushi Patel, F. Stuart Foster, David Goertz, Peter Lee, and Jean Gariépy*

Cite This: *ACS Pharmacol. Transl. Sci.* 2024, 7, 1864−1873

ABSTRACT: Design strategies that lead to a more focused in vivo delivery of functionalized nanoparticles (NPs) and their cargo can potentially maximize their therapeutic efficiency while reducing systemic effects, broadening their clinical applications. Here, we report the development of a noncovalent labeling approach where immunoglobulin G (IgG)-decorated NPs can be directed to a cancer cell using a simple, linear bispecific protein adaptor, termed MFE23-ZZ. MFE23-ZZ was created by fusing a single-chain fragment variable domain, termed MFE23, recognizing carcinoembryonic antigen (CEA) expressed on tumor cells, to a small protein ZZ module, which binds to the Fc fragment of IgG. As a proof of concept, monoclonal antibodies (mAbs) were generated against a NP coat protein, namely, gas vesicle protein A (GvpA) of *Halobacterium salinarum* gas vesicles (GVs). The surface of each GV was therapeutically derivatized with the photoreactive agent chlorin *e*6 (Ce6GVs) and anti-GvpA mAbs were subsequently bound to GvpA on the surface of each Ce6GV. The bispecific ligand MFE23-ZZ was then bound to mAb-decorated Ce6GVs via their Fc domain, resulting in a noncovalent tripartite complex, namely, MFE23.ZZ-2B10−Ce6GV. This complex enhanced the intracellular uptake of Ce6GVs into human CEA-expressing murine MC38 colon carcinoma cells (MC38.CEA) relative to the CEA-negative parental cell line MC38 in vitro, making them more sensitive to light-induced cell killing. These results suggest that the surface of NP can be rapidly and noncovalently functionalized to target tumor-associated antigen-expressing tumor cells using simple bispecific linkers and any IgG-labeled cargo. This noncovalent approach is readily applicable to other types of functionalized NPs.

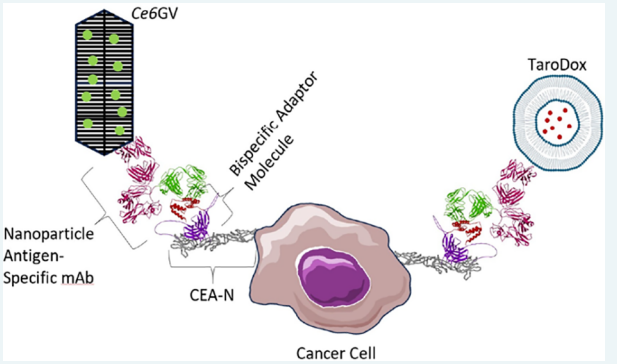

KEYWORDS: *tumor targeting, nanoparticles, adaptor molecule*

INTRODUCTION

One emerging strategy for the delivery of chemotherapeutic reagents is through the use of nanoparticle(s) (NPs). Lipid-based NPs are the most common class of nanomedicine with many formulations currently approved for clinical use.[1] Attributes such as their ease of formulation/modification, biocompatibility, and payload capacity confer selective advantages over classical polymeric and inorganic NPs.[2]

Regardless of the NP used, there is a need to optimally and selectively deliver them to a damaged or inflamed tissue, organ, or at a tumor site to better localize their therapeutic and imaging functions while minimizing adverse off-target effects. Covalently attaching a ligand or antibody to the surface of NPs to target the resulting complex to a diseased cell typically requires the development of case-by-case synthetic coupling approaches. A noncovalent strategy based on the use of a small bispecific protein linker incorporating protein ZZ derived from protein A that generically binds to Fc-containing monoclonal antibodies (mAbs) or protein ligands could prove to be a more adaptable targeting method for labeling a range of NP cargos with distinct functionalities aimed at a common target. For example, one group reported that a ZZ-infused bionanocapsule was able to capture anti-EGFR immunoglobulin G (IgG) and improve its intracellular uptake,[3] while Fornt-Suñé and colleagues created artificial antigen presenting cells by incorporating the Z domain into ZapB coiled coil-based NPs allowing them to be functionalized with anti-CD3 and anti-CD28 antibodies.[4] In another instance, Gil-Garcia and Ventura incorporated the Z domain into α helix-rich bacterial inclusion

Received: March 13, 2024
Revised: May 14, 2024
Accepted: May 23, 2024
Published: June 3, 2024

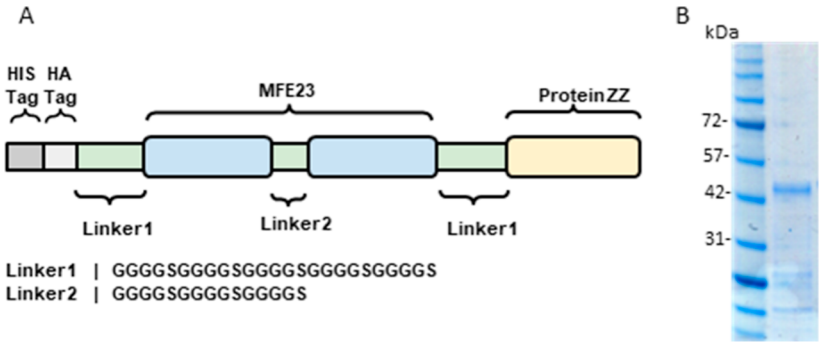

Figure 1. MFE23.ZZ schematic and purity. (A) Schematic representation of the MFE23.ZZ adapter protein construct. The scFv MFE23 binds to the N domain of CEA. This domain was fused using a flexible GS linker to ZZ, an IgG Fc binding protein domain. His and HA tags were incorporated at the N terminus of MFE23 for purification and detection purposes. (B) SDS−PAGE gel of purified MFE23.ZZ protein migrating as a single Coomassie-stained band.

bodies functionalizing them with anti-CD3 and anti-EGFR to localize T-cells to cancer cells.[5]

Here, we report as a proof-of-concept, the development of a small bispecific adaptor protein, termed MFE23-ZZ, that noncovalently links any IgG antibody-decorated cargo and redirects them to the surface of carcinoembryonic antigen (CEA)-expressing tumor cells. Specifically, MFE23, a single-chain fragment variable (scFv) that specifically recognizes the tumor-associated human antigen CEA,[6] was linearly fused to ZZ, a protein A-derived peptide, that binds to Fc domains.[7] We then demonstrate the use of this MFE23-ZZ adapter protein using air-filled *Halobacterium salinarum* gas vesicles (GVs) as a protein-based NP model. GVs are naturally expressed by certain microbes such as *H. salinarum* to regulate their buoyancy in response to stimuli.[8] Their shell is mostly composed of thousands of copies of a single small protein termed gas vesicle protein A (GvpA). GVs can be easily harvested as homogeneous preparations of NPs with a defined size and shape. To date, GVs have been used to deliver peptide-based drugs to treat bacterial infections, transport oxygen to hypoxic tumors, and have served as a carrier for photosensitive drugs such as *chlorin e6* (Ce6GV).[9−11] We have recently generated four mAbs to the *H. salinarum* GvpA protein (Figure S1 and Table S1), one of which (2B10) was selected to create a tripartite noncovalent complex linking MFE23.ZZ to mAb 2B10-decorated Ce6GVs. This homing NP, termed MFE23.ZZ-2B10−Ce6GV, was used to selectively target the surface of MC38.CEA tumor cells, enhancing their phototoxic cell killing function, relative to parental MC38 cells in vitro. This study reports a first example of a broadly applicable, modifiable, noncovalent strategy to deliver antibody-bound NPs to CEA^+ cancer cells.

RESULTS

Generation and Characterization of an MFE23.ZZ Linker and Its Complexation with mAb-Bound *Chlorin e6* (Ce6)-Modified *H. salinarum* Gas Vesicles. We designed and expressed a bispecific protein termed MFE23.ZZ, where MFE23 is a scFv that binds with high affinity to CEA.[6,12] MFE23 was linearly linked to a small protein ZZ domain (11.5 kDa), representing two successive B domains of staphylococcal protein A (Figure 1A). The ZZ domain has been shown to selectively bind to the Fc domain of murine and human IgGs.[13−16] Histidine (His) and hemeagglutinin (HA) tags were inserted at the N-terminus of MFE23.ZZ for purification purposes and the resulting construct expressed in *Escherichia coli* BL-21 cells. MFE23.ZZ was subsequently purified using nickel nitrilotriacetic acid (Ni.NTA) resin. The size and purity of MFE23.ZZ were confirmed by sodium dodecyl−sulfate polyacrylamide gel electrophoresis (SDS−PAGE) (Figure 1B).

The MFE23 domain of MFE23.ZZ retained its binding to CEA displaying a comparable affinity to the one previously reported for MFE23 as evidenced by surface plasmon resonance (SPR) (Table 1).[12]

Table 1. Summary of Binding Constants and Kinetic Parameters for MFE and MFE23.ZZ Binding to the CEA N Domain[a]

CEA N domain	K_d (nM)	k_a 10^4 [M^{-1} s^{-1}]	k_d 10^{-5} [s^{-1}]	chi^2
MFE23	7.2 ± 5	2.1 ± 0.3	1.3 ± 0.1	1.2 ± 1.3
MFE23.ZZ	4.9 ± 0.4	1.5 ± 0.1	7.2 ± 0.1	2.0 ± 1.2

[a]The K_d was determined by single-cycle kinetics using SPR (Biacore T200). Data was analyzed using a 1:1 Langmuir binding model. The values are represented as mean ± standard error of the mean (SEM) from two independent trials.

We have recently developed photoreactive Ce6-modified *H. salinarum* GVs as cytotoxic NPs.[9] These Ce6GVs were used as our model NP in this study. In order to demonstrate that MFE23.ZZ, as a protein linker, is able to selectively bind the IgG Fc domain of antibodies bound to NP, we generated hybridoma cell lines that produce four high-affinity murine mAbs (2B10, 11H12, 11F8, and 13B6) to GvpA. The variable domains of both heavy and light chains of these mAbs were sequenced (Figure S1A) and the presence and integrity of both heavy and light chains were confirmed by SDS−PAGE (Figure S1B). All four mAbs bound with similar low nanomolar affinity to GvpA itself (C-terminus GvpA synthetic peptide used as the immunogen and to full length GvpA [termed GvpA-CaM]), wild-type GVs, and Ce6-GVs as determined by enzyme-linked immunosorbent assay (ELISA) with K_ds ranging from 0.1 to 2.9 nM (Figure S2 and Table S1). The murine IgG2b mAb 2B10 was selected for this study.

The number of GvpA proteins forming one *H. salinarum* surface protein GV shell was previously calculated to be ~55,000.[9] Based on infranatant fluorescence studies, we estimated that ~62,000 fluorescein isothiocyanate (FITC)-labeled 2B10 antibody molecules are bound to a single Ce6-

https://doi.org/10.1021/acsptsci.4c00140
ACS Pharmacol. Transl. Sci. 2024, 7, 1864−1873

modified GV at a 1:1 molar concentration of mAb 2B10 to GvpA (Figure 2 and Table S2).

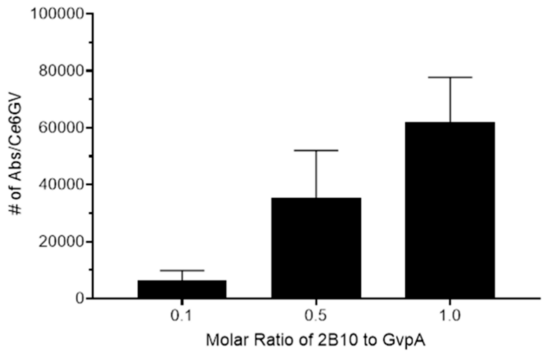

Figure 2. Surface of Ce6GVs is saturated with anti-*H. salinarum* GvpA antibody 2B10 at a 1:1 molar ratio of mAb2B10 to GvpA. The number of GvpA proteins forming one GV shell was previously calculated to be ~55,000.[9] The histogram highlights the calculated number of mAb 2B10 bound to WT GVs or Ce6GVs at 3 different molar ratios of mAb 2B10 to GvpA. Briefly, FITC-labeled 2B10 antibodies were added to a fixed amount of Ce6GVs bound to ELISA plate wells. The level of antibody loading on Ce6GVs was determined from the difference in fluorescence signals between the initial FITC-2B10 antibody added and the residual unbound antibody remaining in solution. Histogram bars represent the calculated mean number of antibodies bound to a single Ce6GV [±standard deviation (SD)] derived from four replicates.

As modeled in Figure 3A, MFE23.ZZ is projected to simultaneously bind to the CEA N domain and the Fc domain of the anti-GvpA mAb 2B10-decorated Ce6GVs (as a complex termed MFE23.ZZ-2B10−Ce6GV). The formation of these complexes was confirmed by performing a bridging ELISA assay (Figure 3B), where the MFE23.ZZ adapter protein simultaneously bound to immobilized 2B10−Ce6GVs and to the CEA N domain. The ability of the MFE23.ZZ adaptor molecule to bind to CEA-expressing MC38.CEA cells but not to CEA$^-$ parental MC38 cells was further confirmed by flow cytometry using a fluorescently labeled murine IgG (bound via the ZZ domain of MFE23.ZZ) (Figure 3C). Importantly, MFE23.ZZ-2B10−Ce6GV complexes remain relatively stable over time in the presence of antibody-containing murine serum, as evidenced by the retention of approximately 35% of such complexes over a 24 h time period (Figure 3D).

Complexes of MFE23.ZZ and 2B10-Bound Ce6GVs Are Readily Internalized and Show Enhanced Phototoxicity toward CEA-Expressing Tumor Cells. We monitored the internalization of Ce6 nanobubbles into CEA$^+$ MC38.CEA cells as reactive oxygen species (ROS) generated by Ce6 upon light exposure is cytotoxic when located near intracellular pools of lipids, proteins, and nucleic acids.[4] Figure 4A shows the time-dependent internalization of MFE23.ZZ-2B10−Ce6GV complexes into MC38.CEA and CEA$^-$MC38 cells at 37 °C. The uptake of MFE23.ZZ-2B10−Ce6GV by MC38.CEA cells reached a plateau after 16 h. In comparison, the internalization of untargeted Ce6GVs peaked at half the maximal MFI values observed for MFE23.ZZ-2B10−Ce6GVs over time. In contrast, the uptake of MFE23.ZZ-2B10−Ce6GVs by the parental CEA$^-$ MC38 cell line was significantly reduced and comparable to untargeted Ce6GVs at 37 °C (Figure 4A). As expected, the internalization by either cell line of targeted and untargeted Ce6GVs was blocked at 4 °C (Figure S3).

Additionally, MC38.CEA and MC38 cells were exposed for up to 24 h to increasing concentrations of untargeted Ce6GVs or MFE23.ZZ-2B10−Ce6GVs normalized to an equivalent molar dose of Ce6 or an equivalent amount of WT GVs. The GV-loaded cells were exposed to a 660 nm light source for 10 min to activate Ce6. Cell viability was measured 24 h later using the colorimetric water-soluble tetrazolium salt (WST-1) assay. Cell viability decreased in a concentration-dependent manner upon light exposure for both MC38 and MC38.CEA cells that were pretreated with Ce6GVs or MFE23.ZZ-2B10−Ce6GV (Figure 4B). Of note, light exposure in the absence of Ce6 is not expected to have an effect on the viability of cells.[17] As expected, the cytotoxic effect (as reflected from calculated CD_{50} values) of MFE23.ZZ-2B10−Ce6GVs was 13.6 times greater than that observed for untargeted Ce6GVs toward MC38.CEA cells (Figure 4B). Additionally, this enhancement in light-activated cell killing was not observed for CEA$^-$ MC38 parental cells nor did wild-type GVs cause any cell toxicity. This enhanced cytotoxic activity correlated with an increase in intracellular ROS (Figure 4C). The light-induced ROS production was measured using 2, 7-dichlorofluorescein diacetate (DCF-DA). Levels of cellular ROS generated by MC38.CEA cells loaded with MFE23.ZZ-2B10−Ce6GV were twofold greater than ROS levels arising from Ce6GVs alone in MC38.CEA cells. As anticipated, no significant difference was observed in ROS levels in parental MC38 cells treated with CEA-targeted or -untargeted Ce6GVs. Furthermore, no significant changes in cytotoxicity or production of ROS were noted for either cell line in the absence of light (Figure 4B,C). Collectively, these results highlight the selective and therapeutic advantage of using MFE23.ZZ-2B10−Ce6GV to target and kill CEA-expressing tumor cells in vitro.

DISCUSSION

We recently reported the successful coupling of the photoreactive Ce6 to the surface of GVs.[9] These naturally occurring air-filled protein NPs presently lack any targeting function that would allow them to accumulate in specific organs, tissues, or near tumor cells in vivo. As in the case of most NPs, covalently modifying their surface with ligands such as antibodies while maintaining the integrity of such particles as well as their cargo can prove to be challenging. To circumvent this issue, we have devised a simple, broadly applicable, noncovalent strategy, that does not require chemical coupling of a ligand to the particle surface, to selectively target NPs to any desired antigen. The key to our strategy is a short bispecific adaptor protein incorporating two ligands, namely, a specific scFv, against a desired cell surface target antigen, on the N terminus and the IgG-binding ZZ peptide on the C terminus, capable of binding to any Fc-containing protein, for example, a mAb that binds to a surface determinant on a NP.

Specifically, we constructed the linear adapter protein MFE23.ZZ incorporating a CEA-specific scFv (MFE23)[6] on its N terminus linked to the ZZ protein peptide on its C terminus (Figure 1A). CEA is an established tumor-associated antigen that is frequently overexpressed by several types of epithelial cancers including colorectal, gastric, pancreatic, breast, and small cell lung cancers.[18] MFE23.ZZ was shown to bind to CEA with an affinity constant in the nanomolar range as observed for MFE23 alone (Table 1).[12]

https://doi.org/10.1021/acsptsci.4c00140
ACS Pharmacol. Transl. Sci. 2024, 7, 1864−1873

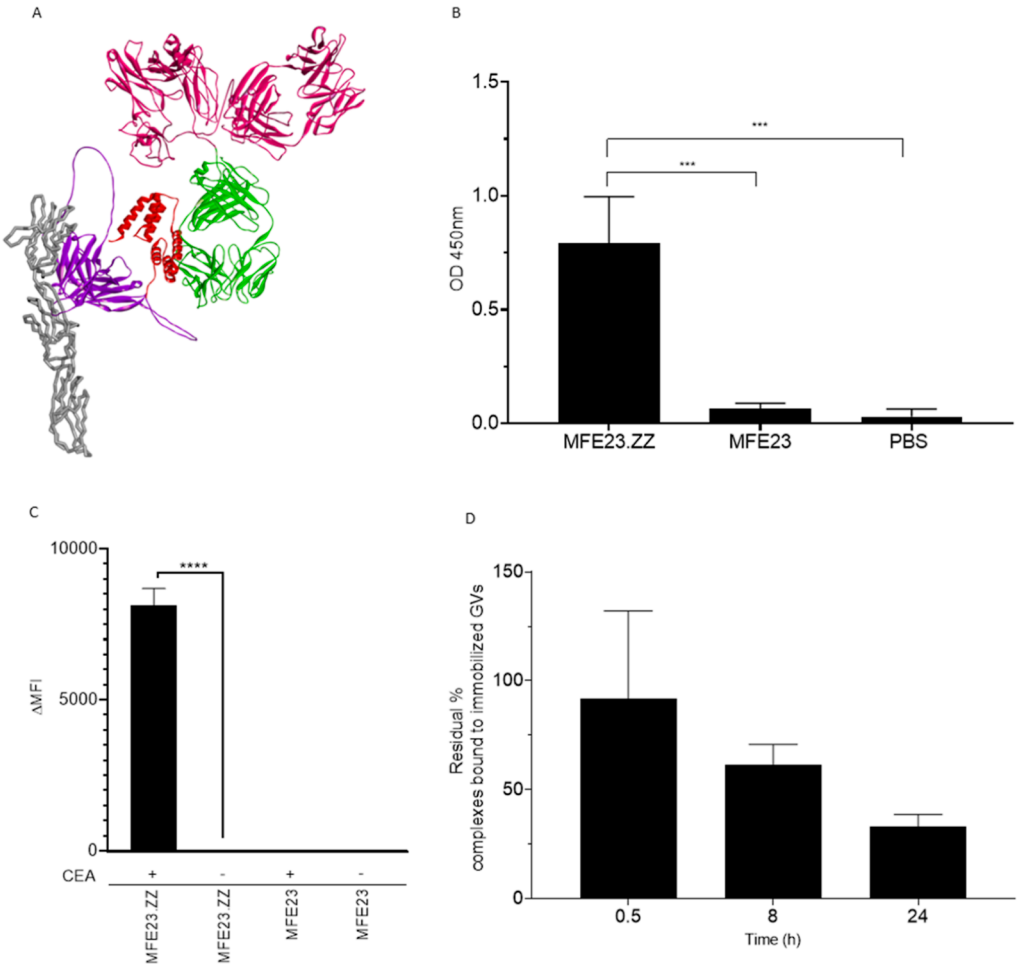

Figure 3. The MFE23.ZZ adapter protein can bind simultaneously to C*e*6GVs and the CEA N domain. (A) Ribbon model of a tripartite complex composed of the bispecific MFE23.ZZ adapter protein (purple and red domains, respectively) bound to the IgV-like N domain (in gray) of CEA and to the Fc domain (in green) of an antibody. The predicted ribbon representation of the tripartite complex (Dassault Systèmes BIOVIA Discovery Studio 2020 Visualizer) was generated using Google DeepMind AlphaFold and pdb structures of CEA, MFE.23, ZZ domain, and IgG1. (B) Bar diagram of bridging ELISA results showing that the MFE23.ZZ adapter protein can dually bind C*e*6GVs and the CEA N domain. ELISA plate wells were coated with C*e*6GVs. The anti-GvpA antibody 2B10 was then dispensed into wells followed by the addition of MFE23.ZZ or MFE23 or PBS. MFE23.ZZ-2B10−C*e*6GV complexes were detected by adding the purified CEA N domain to each well and by detecting the bound CEA domain with a rabbit polyclonal anti-CEA antibody followed by an antirabbit antibody-HRP conjugate (n = 6, one-way ANOVA with Tukey's multiple-comparison test; $p \leq 0.001$, ***). (C) MFE23.ZZ is able to simultaneously bind to CEA on CEA^{+}MC38.CEA cells and to a murine IgG2b mAb. Murine colorectal MC38.CEA or parental CEA^{-} MC38 cells were incubated with either MFE23.ZZ, MFE23 alone, or without construct. Cells were subsequently incubated with a fluorescent murine IgG2b-APC-Cy7 conjugate to identify by flow cytometry if the adapter protein MFE23.ZZ can simultaneously associate with full length CEA on MC38.CEA cells and a murine IgG Fc domain. The bar diagram depicts the difference in mean fluorescence intensities (ΔMFIs) values calculated by subtracting the MFI from MC38 or MC38.CEA cells incubated with IgG2b-APC-Cy7 alone from the appropriate cell line incubated with the indicated construct. Each bar represents the average ΔMFI ± SD derived from four replicates (n = 4, unpaired t test; $p \leq 0.0001$, ****) (D) MFE23.ZZ-2B10−C*e*6GV complexes are stable in mouse serum. The mAb 2B10 was dispensed into ELISA plate wells precoated with C*e*6GVs. MFE23.ZZ was subsequently added into wells containing the immobilized 2B10−C*e*6GV complexes. The resulting trimolecular complexes were then exposed to murine serum for either 0.5, 8, or 24 h at 37 °C to assess the displacement of mAb 2B10 by murine serum antibodies from the plate-bound C*e*6GV complexes over time. Residual MFE23.ZZ-2B10 antibody complexes bound to immobilized C*e*6GVs were detected using the purified CEA N domain protein, followed by a rabbit polyclonal anti-CEA antibody and a goat polyclonal antirabbit IgG Fc antibody conjugated to HRP. Each bar represents the average percentage of MFE23.ZZ bound to mAb 2B10 ± SD derived from three replicates.

The second key component of this proof-of-concept study was to develop mAbs against the surface determinant GvpA, the dominant surface protein forming the *H. salinarum* GV shell with a view to have the ZZ domain of MFE.ZZ bind to their Fc domain. We generated several high affinity mAbs to GvpA (Figure S1 and Table S1). Clone 2B10 was of particular interest as it bound tightly to C*e*6GVs with a low nM K_d comparable to that observed for the peptide immunogen used (GvpA synthetic peptide corresponding to the C-terminal, solvent-exposed α-helix of *H. salinarum* GvpA)[19] as well as the full-length GvpA protein (Figure S2 and Table S1). Furthermore, mAb 2B10 saturated the surface of *H. salinarum* GVs with up to 62,000 antibodies bound per GV (Figure 2 and Table S2). Interestingly, the GvpA peptide used as our immunogen is also present in GVs produced by other halophilic archaeal species including *Nitrosomonas* sp. LN261, *Salarchaeum* sp. JOR-1, and *Haloferax meditterania*,

https://doi.org/10.1021/acsptsci.4c00140
ACS Pharmacol. Transl. Sci. 2024, 7, 1864−1873

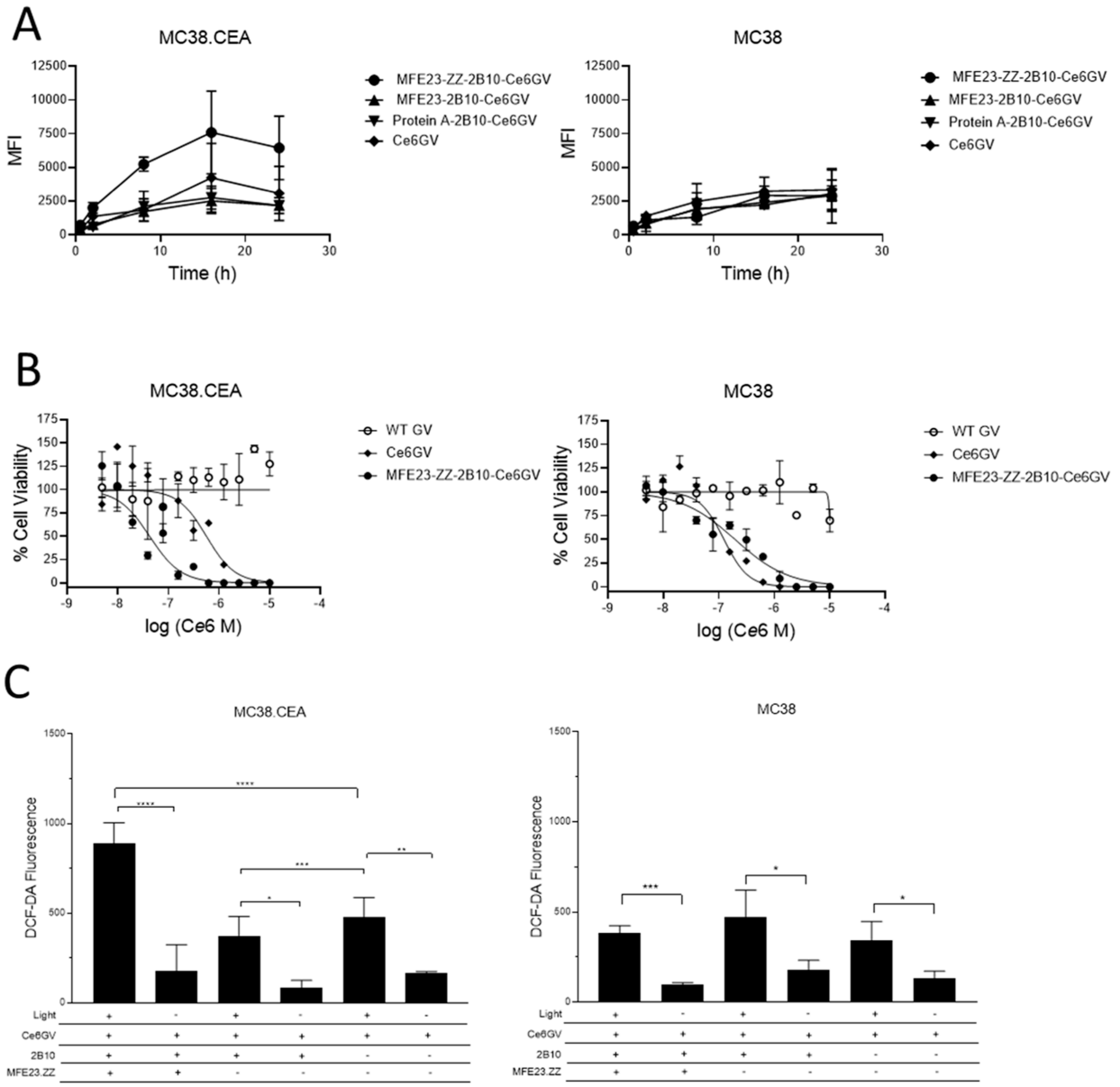

Figure 4. In vitro functional characterization of MFE23.ZZ-2B10−C*e*6GVs. (A) Time-dependent internalization of targeted or untargeted C*e*6GVs into CEA$^+$ MC38.CEA and CEA$^-$ MC38 cells. Ce6GVs were precomplexed with anti-*H. salinarum* GvpA antibody 2B10 and MFE23.ZZ, or with anti-GvpA antibody and protein A, or 2B10 and MFE23 lacking the ZZ domain or C*e*6GVs alone. Targeted or untargeted C*e*6GV formulations were incubated with murine CEA$^+$MC38.CEA or CEA$^-$MC38 cells over a 24 h period at 37 °C. The cellular uptake of C*e*6GVs and their complexes was monitored by detecting C*e*6 fluorescence in cells by flow cytometry. Each data point represents the average MFI ± SD derived from four replicates. No cellular uptake was observed at 4 °C (Figure S2). (B) Cell viability upon light exposure of MC38.CEA or MC38 cells treated with CEA-targeted or -untargeted C*e*6GVs. MC38.CEA or MC38 cells were pretreated for 24 h with either MFE23.ZZ-2B10−C*e*6GVs, C*e*6GVs, or WT GVs, subsequently exposed to 660 nm light for 10 min and incubated for an additional 24 h before determining their viability (WST-1 assay). Each data point represents the mean percent cell viability ± SD derived from six replicates. (C) Assessment of the relative levels of ROS generated in MC38.CEA and MC38 cancer cells treated with targeted or untargeted C*e*6GVs in the presence or absence of light exposure. MC38.CEA or MC38 cells were treated with C*e*6GVs alone, 2B10−C*e*6GV complexes, or MFE23.ZZ-2B10−C*e*6GV complexes for 8 h to permit internalization. The intracellular production of singlet oxygen species upon light irradiation was detected by flow cytometry (fluorescein channel) using DCF-DA. Each bar represents the average MFI ± SD (n = 4, one-way ANOVA with Tukey's multiple-comparison test), $P \leq 0.05$*, $P \leq 0.01$**, $P \leq 0.001$***, $P \leq 0.0001$****.

suggesting that the current repertoire of mAbs could potentially recognize other types of GVs.

The overall objective of this study was to use MFE23.ZZ as an adaptor molecule to preferentially target mAb 2B10-saturated C*e*6GVs[9] to CEA-expressing colon carcinoma (MC38.CEA) cells. The bispecific construct MFE23.ZZ, as depicted in Figure 3A, was expected to form a noncovalent bridge between CEA and the Fc domain of mAb 2B10-decorated C*e*6GVs. Previous groups have shown that pro-urokinase or photoprotein ZZ fusion constructs maintain their binding to IgGs.[20−25] mAb 2B10 was no exception. MFE23-ZZ was able to simultaneously capture the CEA N domain and mAb 2B10-bound GVs forming the tripartite complex MFE23.ZZ-2B10−C*e*6GVs as evidenced using a bridging

https://doi.org/10.1021/acsptsci.4c00140
ACS Pharmacol. Transl. Sci. 2024, 7, 1864−1873

ELISA (Figure 3B) and by flow cytometry using CEA$^+$ MC38.CEA cells (Figure 3C).

We then monitored the binding and internalization of Ce6 nanobubbles into CEA$^+$ MC38.CEA cells at 37 °C (Figure 4A) over time. The uptake of MFE23.ZZ-2B10−Ce6GV by MC38.CEA cells reached a plateau after 16 h. In comparison, the internalization of untargeted Ce6GVs peaked at half the maximal MFI values observed for MFE23.ZZ-2B10−Ce6GVs over the same time period. Furthermore, the uptake of MFE23.ZZ-2B10−Ce6GVs by the parental CEA$^-$ MC38 cell line was significantly reduced and comparable to untargeted Ce6GVs. The levels of Ce6GV internalization observed among the nontargeted controls are comparable to the nonspecific uptake levels of Ce6GV NPs by macropinocytosis previously reported by us for other cancer cell lines.[9] Other CEA-targeted constructs such as MFE23-G2 carboxypeptidase fusion and MFE23-prodrug linamarin conjugate displayed a similar enhancement in uptake in CEA$^+$ LS174T tumors as compared to their nontargeted control.[22,23]

In terms of the therapeutic potential of these complexes, we have previously shown that untargeted Ce6GVs are moderately taken up by human breast MCF-7 and human hypopharyngeal FaDu-GFP cancer cells, resulting in a 200-fold increase in toxicity as compared to the free drug.[9] In light of the increased uptake observed for MFE23.ZZ-2B10−Ce6GVs, we observed a 13.6 times greater cytotoxic effect MFE23.ZZ-2B10−Ce6GVs on MC38.CEA cells relative to the untargeted Ce6GVs (Figure 4B). Additionally, this enhancement in light-activated cell killing was not observed for CEA$^-$ MC38 parental cells. This heightened cytotoxic activity correlated with a twofold increase in the production of intracellular ROS upon light activation. Once produced, intracellular ROS elicit their toxic effect by locally damaging cellular and organellar lipids and proteins to trigger apoptosis.[26] No significant change in cytotoxicity or production of ROS was noted for either CEA$^+$ or CEA$^-$ cell lines in the absence of light (Figure 4C). Collectively, these results highlight the selective and therapeutic advantage of using MFE23.ZZ-2B10−Ce6GV to target and kill CEA-expressing tumor cells in vitro. It should be noted that while Ce6 has several desirable properties for photodynamic therapy,[27−31] in vivo preclinical studies involving in situ tumors would likely be better served using different photodynamic reagents, namely, chromophores activated by longer wavelengths of light allowing for enhanced depth of penetration (up to 5 cm).[31] IR825 is a cyanine derivative and one example of a near-infrared light-absorbing drug that could be explored.[32]

From a current clinical perspective, liposomal scaffolds represent the highest proportion of NP drug formulations used in the clinic and/or clinical trials.[33] Targeting these drug formulations, however, remains a challenge. For instance, the initial preclinical testing of an HER2-targeted pegylated liposomal doxorubicin formulation showed synergistic antitumoral activity when used in combination with Trastuzumab in HER2-overexpressing xenograft models of breast and gastric cancer.[34] However, a subsequent Phase II trial (NCT02213744) was halted due to the lack of clinical benefit over controls.[35] Unsurprisingly, our preliminary attempt at using the anti-PEG humanized 6.3 antibody[36,37] in combination with MFE23-ZZ resulted in the successful formation of a tripartite complex (MFE23.ZZ-6.3-TaroDOXOrubicin) incorporating the pegylated liposomal doxorubicin. MFE23.ZZ-6.3-TaroDOXOrubicin complex was shown to bind the CEA N domain using a bridging ELISA assay (Figure S4A). However, coinciding with the clinical trial (NCT02213744), we did not observe in our in vitro assay that this approach conferred a significant advantage over the control in targeting TaroDOX-Orubicin to the surface MC38.CEA cells as evidenced by flow cytometry (Figure S4B). This result suggests that TaroDOX-Orubicin liposomes may nonspecifically stick to cells, particularly those expressing CEA on the surface, given the overall higher signal observed as compared to MC38 cells not expressing CEA. The MFE23.ZZ adaptor molecule, however, can be readily re-engineered to incorporate an alternate scFv or antigen binding modality, directed toward other surface antigens of interest, and would likely be necessary in combination with an alternative cell line to investigate the potential of this strategy to effectively target clinically relevant TaroDOXOrubicin to the surface of cells.

In conclusion, we have devised a simple strategy to spontaneously assemble tumor-targeted tripartite NP complexes composed of a CEA-targeted adapter protein (MFE23.ZZ) recognizing the Fc domain of an anti-*H. salinarum* GvpA antibody (2B10) bound to Ce6GVs. This proof-of-concept study applying the MFE23-ZZ adaptor molecule is just one example of marker-targeted adapter designs containing Fc-binding generic ZZ domains. This noncovalent MFE23.ZZ antibody-targeting system may be rapidly adapted for use with a range of other lipid and solid NPs for which mAbs are available.

MATERIALS AND METHODS

Generation of MFE23-ZZ Bispecific. MFE23.ZZ was constructed by fusing a scFv against the CEA N domain[6] to protein A-derived peptide ZZ.[7] The genes coding for MFE23.ZZ and MFE23 (serving as a control) were cloned into pET 302 plasmids, which included a hexahistidine tag (GeneArt; Thermo Fisher Scientific). Both constructs were expressed in *E. coli* One Shot BL-21 (DE3) (Thermo Fisher Scientific). Transformants were grown in lysogeny broth (LB; Millipore Sigma) with ampicillin (BioShop Canada Inc.) (100 μg/mL) at 37 °C. Following isopropyl β-D-1-thiogalactopyranoside (IPTG; Millipore Sigma) (1 mM) induction, cultures were shaken overnight at room temperature, pelleted, and lysed (phosphate buffered saline (PBS; Wisent) pH 7, 1% triton-X-100 (Millipore Sigma), 500 μL protease inhibitor cocktail (Millipore Sigma), 1 μL benzonase nuclease (Millipore Sigma), and 1 mg/mL lysozyme (Millipore Sigma)). The cleared lysates were then centrifugated (14,000*g*, 15 min, 4 °C) and the pellets were resuspended in a denaturing buffer (6 M urea (Millipore Sigma), 500 mM NaCl (Millipore Sigma), and 50 mM Tris−HCl (Millipore Sigma)) and sonicated in a water bath for 20 min. Following centrifugation, MFE23.ZZ- and MFE-containing supernatants were loaded onto a Ni^{2+} NTA (Thermo Fisher Scientific) column to recover each protein. The eluted proteins were desalted using PD-10 columns (Cytiva). Their purity was confirmed by SDS−PAGE.

Generation of Monoclonal Anti-*H. salinarum* GvpA Antibodies. Hybridomas producing monoclonal anti-*H. salinarum* GvpA antibodies were generated by GenScript (New Jersey, USA) by immunizing mice with a 26-residue synthetic peptide (FLHYAEEIAKIEQAELTAGAEAAPEA) corresponding to the C-terminal solvent-exposed α-helix of GvpA[19] fused to keyhole limpet hemocyanin. Hybridomas were adapted to growth in H-CELL serum-free medium

https://doi.org/10.1021/acsptsci.4c00140
ACS Pharmacol. Transl. Sci. 2024, 7, 1864−1873

(Wisent) for mAb production. mAbs were purified from culture supernatants using affinity chromatography on protein A-sepharose beads (Thermo Fisher Scientific). Briefly, the supernatants were passed through the protein A-sepharose beads twice, followed by a wash step with PBS pH 7. The bound antibodies were eluted using 0.2 M glycine (Millipore Sigma) pH 2 and the eluted fraction was neutralized using 3 M Tris−HCl pH 8. Each eluted antibody was finally buffer exchanged into PBS using PD-10 columns. The purity of both heavy and light chains for all 4 mAbs was confirmed by SDS−PAGE.

Sequencing of Anti-*H. salinarum* GvpA Monoclonal Antibodies. The mAb variable domain sequences were determined by Sanger sequencing as previously described.[10] Briefly, phenol−chloroform RNA extraction was performed on >2 × 10^6 hybridoma cells treated with the TRIzol reagent (Thermo Fisher Scientific). cDNA was synthesized from the RNA using the SensiFAST cDNA synthesis kit (Bioline/FroggaBio) in accordance to the manufacturer's instructions. The heavy and light chain variable sequence regions were then amplified by touchdown polymerase chain reaction (PCR) using murine isotype-specific primers.[38] PCR products were treated with the ExoSAP-IT express PCR product cleanup kit (Thermo Fisher Scientific) and sent in for Sanger sequencing at the Center for Applied Genomics (Hospital for Sick Children, Toronto, ON, Canada). Sequences were aligned against the IMGT database[39] using IgBlast (www.ncbi.nlm.nih.gov/igblast/; National Center for Biotechnology Information, Bethesda, MD, USA).[40] Alignment was completed using Clustal Omega (https://www.ebi.ac.uk/Tools/msa/clustalo/; EMBL-EBI, Hinxton, Cambridgeshire, UK).[41]

Quantification of Antibody Loading on GVs. Exposed amino groups of a representative anti-*H. salinarum* GvpA antibody (2B10) were covalently modified with FITC (Millipore Sigma) as per the manufacturer's instructions. The level of antibody loading on GVs and C*e*6-GVs was then estimated using FITC-labeled mAb 2B10. Increasing concentrations of 2B10-FITC were added to 10 μg of GVs or C*e*6-GVs in suspension and incubated overnight at room temperature. The fluorescence of the infranatant was compared to a standard curve of 2B10-FITC (λ_{ex} 490 nm and λ_{em} 525 nm) as a function of 2B10 antibody concentration. The quantity of the unbound antibody was subtracted from the initial quantity of antibodies added to estimate the level of antibody loading.

SPR. The binding of MFE23.ZZ to the CEA N domain (the antigen recognized by MFE23) was confirmed using SPR (Biacore T200, GE Healthcare). A biotin-labeled recombinant form of the CEA N domain (residues 1−132) was immobilized onto a streptavidin-coupled chip (Cytiva). MFE23.ZZ, MFE23, or protein A (BioVision) was then injected at increasing concentrations (12.5, 25, 50, 100, and 200 nM) using a flow rate of 50 μL/min for a contact period of 240 s and a dissociation period of 2400 s. Protein solutions were diluted in 4-(2-hydroxyethyl)-1-piperazineethanesulfonic acid (HEPES) buffered saline (HBS-EP+) pH 7.4 buffer (0.01 M HEPES (Millipore Sigma), 0.15 M NaCl (Millipore Sigma), 3 mM ethylenediaminetetraacetic acid (EDTA; Wisent), and 0.005% Tween-20 (Millipore Sigma)). The chip was regenerated using a Biacore Regeneration solution (pH 1.7) (Cytiva) after each dissociation step. Binding curves were constructed and fitted using a 1:1 Langmuir binding model. Reported binding parameters were values derived from two independent SPR experiments.

Generation of Anti-PEG Humanized 6−3 Antibody. The anti-PEG humanized 6−3 antibody (hIgG4) was constructed based on the reported sequences by Roffler and colleagues.[36,37] The gene was cloned into a pcDNA 3.4 TOPO vector (GeneArt; Thermo Fisher Scientific). The resulting recombinant antibody was expressed in Expi293 cells and purified by protein A affinity chromatography as described above.

Bridging ELISA. To determine if the mAbs could bind intact GVs, 0.5 μg/well of WT GVs or therapeutically relevant GVs modified with C*e*6 in PBS were coated in a 96-well ELISA plate (Corning) overnight at room temperature. The plate was blocked for 1 h at room temperature using 1% bovine serum albumin (BSA; BioShop Canada Inc.). Increasing concentrations of each monoclonal anti-*H. salinarum* GvpA antibody were dispensed into wells and incubated for 1 h at 37 °C. Bound antibodies were detected using a polyclonal goat antimouse IgG Fc-horse radish peroxidase (HRP) conjugate (Bethyl Laboratories).

A bridging ELISA was performed to determine if MFE23.ZZ could simultaneously bind to mAb 2B10-bound Ce6GV and to CEA. Here, ELISA plate wells were coated overnight with C*e*6GVs (5 μg/mL) at room temperature (25 °C). The wells were washed and blocked with 1% BSA for 1 h at room temperature. mAb 2B10 (100 μL; 400 nM) was then dispensed into wells for a 1 h incubation at 37 °C, followed by MFE23.ZZ or MFE23 for 1 h at 37 °C. Wells were then washed three times. The CEA N domain (in house) (100 μL; 400 nM) was then added into wells. After 1 h at 37 °C, binding was detected using a rabbit polyclonal anti-CEA antibody (Dako), followed by an antirabbit antibody conjugated to HRP (Bethyl Laboratories). The substrate TMB was added and optical density was recorded at 450 mm. Average optical density measurement ± SD values were derived from experiments performed in triplicate.

Similarly, a bridging ELISA was performed to determine if MFE23.ZZ could simultaneously bind to a humanized dimeric (grafted to hIgG4 scaffold) anti PEG scFv; 6.3-Fc[37] bound to TaroDOXOrubicin (Taro Pharmaceutics Inc., Ontario, Canada) and CEA. Here, wells were coated with TaroDOX-Orubicin (0.5 μg/well) in a 96-well ELISA plate overnight at room temperature. The plate was blocked for 1 h at 37 °C with 1% BSA. The scFv 6.3-Fc (5 μg/mL) or an irrelevant antibody (mAb 8G10)[42] (regrafted to a human IgG4; in house) was added to the wells, followed by 5 μg/mL of MFE23.ZZ and the biotinylated CEA N domain. Each incubation was for 1 h at 37 °C. Successful complexes were detected using streptavidin HRP (Millipore Sigma).

All ELISAs were developed using a 3,3′,5,5′-tetramethylbenzidine (TMB) liquid substrate (Molecular Innovations) and optical density was recorded at 450 mm using a microplate reader (Synergy H1). Average optical density measurement ± SD values were derived from experiments performed in triplicate.

Cell Lines. MC38.CEA and CEA parental MC38 murine colon carcinoma cell lines, kindly provided by Dr. J. Schlom (National Cancer Institute; Bethesda, Maryland), were used in this study. Both cell lines were cultured at 37 °C in a humidified 5.0% CO_2 atmosphere in Dulbecco's modified Eagle's medium (DMEM; Wisent) supplemented with 10%

https://doi.org/10.1021/acsptsci.4c00140
ACS Pharmacol. Transl. Sci. 2024, 7, 1864−1873

FBS, penicillin (100 U/mL)/dihydrostreptomycin (100 μg/mL) (Wisent).

Displacement Analysis of MFE23.ZZ Complexed to Anti-Gvpa mAb 2B10 by Serum IgG. 2B10 mAb complexed to MFE23.ZZ was exposed to murine serum to assess the displacement of 2B10 by serum IgGs over time. ELISA plates (Corning #9018) were coated overnight at room temperature with Ce6GVs (5 μg/mL). After blocking, wells were then washed and 2B10 (400 nM) was added for a 1 h incubation at 37 °C. MFE23.ZZ (400 nM) was subsequently added to wells for a 1 h incubation at 37 °C. Murine serum (Abcam, ab7486) was added to compete with 2B10 for binding to MFE23.ZZ. Wells receiving no serum (PBS only) served as controls. The plate-bound antibodies were incubated with serum at 37 °C for 0.5, 8, and 24 h. Residual 2B10 bound to MFE23.ZZ was then detected as described above.

Time-Dependent Binding and Internalization of MFE23.ZZ-2B10 Complexes into Cancer Cells. Fluorescent Ce6GVs were precomplexed with 2B10 and MFE23.ZZ, MFE23, or protein A for 1 h at room temperature. The resulting floating complexes were purified using two rounds of centrifugation-flotation steps. MC38.CEA and MC38 cells (10^6 cells) were seeded into 12-well tissue culture plates and incubated overnight. Targeted or untargeted Ce6GVs (0.5 μg/mL Ce6; 1 mL DMEM (Gibco)) or native GVs (equivalent GV concentration in the Ce6GVs) were then dispensed into cell-containing wells. Plates were then maintained at 4 or 37 °C under continuous rotation. Cells from wells were retrieved at selected time points (0.5 to 24 h) to assess cell viability and the internalization of GV complexes by flow cytometry. Briefly, well-bound cells were trypsinized using Trypson−EDTA (Wisent), washed with PBS once, and stained with 4′,6-diamidino-2-phenylindole (DAPI; Thermo Fisher Scientific). Cellular uptake of Ce6 was measured by flow cytometry (BD LSR II flow cytometer (BD) maintained by The Center for Flow Cytometry and Scanning Microscopy (CCSM) at the Sunnybrook Research Institute (SRI; Sunnybrook Health Sciences Center, Toronto, ON, Canada) as median fluorescence intensity (MFI) (λ_{exc} 405 nm). Similarly, targeted (using 6.3 in place of 2B10) or untargeted TaroDOXOrubicin (2.5 μg/mL) was dispensed into cell-containing wells. Plates were maintained at 37 °C and cells were subsequently harvested at selected time points. TaroDOXOrubicin accumulation at the surface of the cell was detected using flow cytometry (λ_{exc} 470 nm).

Cell Viability Measurements Following Treatment with MFE23.ZZ-2B10 Complexes. The viability of MC38.CEA and MC38 cells exposed to targeted or untargeted photoreactive Ce6 complexes was measured using the tetrazolium salt-based WST-1 cell proliferation assay. Briefly, cells were seeded (10^5 cells per well in DMEM with 10% FBS) into 96-well plates and incubated overnight at 37 °C (5% CO_2). Cells were then treated with serial dilutions of either MFE23.ZZ-2B10−Ce6GV, Ce6GV, or WTGV normalized to the equivalent Ce6 or WT GV molar dose for 24 h at 37 °C. Cells were then washed and exposed to a light-emitting diode (LED) light source (660 nm, 15−35 mW/cm^2; ABI 25 W Deep Red) for 10 min. Following light treatment, cells were incubated for 24 h at 37 °C in the dark. The medium was then removed and 10 μL of the WST-1 reagent (Roche) in 90 μL of growth medium was added to each well. After 24 h, absorbance readings at 480 nm were recorded using a microplate reader (Synergy H1). Cell viability was normalized relative to a positive control (50 μg/mL Doxorubicin HCl (Pfizer) treatment leading to complete cell death) and a negative control (untreated cells) using the following equation

$$(\text{absorbance sample} - \text{absorbance positive control})/(\text{absorbance negative control} - \text{absorbance positive control}) \times 100\%$$

In Vitro Intracellular ROS Generation Assay. DCF-DA (Millipore Sigma) was used to detect intracellular ROS. DCF-DA is deacetylated upon internalization to become 2′,7′-dichlorofluorescein (fluorescent) upon oxidation with ROS.[43] For this assay, cells were seeded overnight into 24-well plates (5×10^5 cells). The next day, cells were treated for 8 h with Ce6GVs or with Ce6GVs precomplexed with either 2B10 and MFE23.ZZ, or protein A or MFE23 (each adjusted to 0.5 μg/mL Ce6), or with WTGVs (equivalent GV dose). Cells were washed and then exposed either to light (660 nm) for 10 min or kept in the dark. DCF-DA (5 μM) was subsequently added and cells were left for 30 min at 37 °C. Cells were then washed twice in the dark, trypsinized, and stained with DAPI. Cytometric analyses of residual viable cells were monitored based on their DAPI staining pattern (λ_{exc} 405 nm, BP filter 450−50 nm). The MFI values from the DCF fluorescence signal (λ_{exc} 488 nm, BP filter 500−50 nm) were monitored in parallel by flow cytometry.

Modeling of MFE23.ZZ Bound to Its Ligands. A predicted ribbon representation of MFE23.ZZ bound to the CEA N domain and to an IgG Fc domain (Dassault Systèmes BIOVIA Discovery Studio 2020 Visualizer) was generated using GoogleDeepMindAlphafold[44] (https://colab.research.google.com/github/Fbosokrypton/ColabFold/blob/main/beta/AlphaFold2_advanced.ipynb) derived from a stepwise series of overlaps and structure superimpositions of the published structures: CEA (pdb id:1E07) and MFE-23 (pdb id:1QOK),[45,46] a mouse IgG1 monoclonal antibody (pdb id: 1IGY) to represent mAb 2B10,[47] and a crystal structure of the Z domain of staphylococcal protein A bound to an IgG Fc region (pdb id: 5U4Y).[48]

Statistical Analysis. Data were analyzed using GraphPad Prism 8.0 (GraphPad Software, La Jolla, CA, U.S.A.). *P* value of less than 0.05 was considered significant. The statistical significance between 2 groups was determined using a two-tailed student *t* test, whereas statistical analyses between more than 2 groups were determined using a one-way ANOVA with multiple-comparison test or a two-way ANOVA multiple-comparison test. An asterisk represents statistical significance as follows: $*P < 0.05$, $**P < 0.01$, $***P < 0.001$, $****P < 0.0001$. All data are presented as mean values ± SD, and the number of independent experiments (*n*) is listed within the figure legend.

■ ASSOCIATED CONTENT

Supporting Information

The Supporting Information is available free of charge at https://pubs.acs.org/doi/10.1021/acsptsci.4c00140.

The plasmid construct encoding MFE23.ZZ has been deposited at Addgene. Characterization of the four murine monoclonal anti-*H. salinarum* GvpA antibodies, murine monoclonal anti-H. salinarum GvpA antibodies displaying high affinity toward four distinct forms of the

https://doi.org/10.1021/acsptsci.4c00140
ACS Pharmacol. Transl. Sci. 2024, 7, 1864−1873

GvpA antigen, summary of binding constants for anti-GvpA antibodies, Ce6-labeled GVs, time-dependent internalization of targeted or untargeted Ce6GVs at 4°C, bar diagram of MFE23.ZZ-6.3 TaroDOXOrubicin bridging ELISA results, and targeting TaroDOXOrubicin to the surface of MC38.CEA cells.(PDF)

AUTHOR INFORMATION

Corresponding Author

Jean Gariépy − *Physical Sciences, Sunnybrook Research Institute, Toronto, Ontario M4N 3M5, Canada; Department of Pharmaceutical Sciences, University of Toronto, Toronto, Ontario M5S 3M2, Canada; Department of Medical Biophysics, University of Toronto, Toronto, Ontario M5G 1L7, Canada*; Email: jean.gariepy@utoronto.ca

Authors

Ann Fernando − *Physical Sciences, Sunnybrook Research Institute, Toronto, Ontario M4N 3M5, Canada; Department of Pharmaceutical Sciences, University of Toronto, Toronto, Ontario M5S 3M2, Canada*

Amanda Sparkes − *Physical Sciences, Sunnybrook Research Institute, Toronto, Ontario M4N 3M5, Canada;* orcid.org/0009-0008-2453-6818

Esther I. Matus − *Physical Sciences, Sunnybrook Research Institute, Toronto, Ontario M4N 3M5, Canada; Department of Medical Biophysics, University of Toronto, Toronto, Ontario M5G 1L7, Canada*

Ayushi Patel − *Physical Sciences, Sunnybrook Research Institute, Toronto, Ontario M4N 3M5, Canada*

F. Stuart Foster − *Physical Sciences, Sunnybrook Research Institute, Toronto, Ontario M4N 3M5, Canada; Department of Medical Biophysics, University of Toronto, Toronto, Ontario M5G 1L7, Canada*

David Goertz − *Physical Sciences, Sunnybrook Research Institute, Toronto, Ontario M4N 3M5, Canada; Department of Medical Biophysics, University of Toronto, Toronto, Ontario M5G 1L7, Canada*

Peter Lee − *Physical Sciences, Sunnybrook Research Institute, Toronto, Ontario M4N 3M5, Canada*

Complete contact information is available at: https://pubs.acs.org/10.1021/acsptsci.4c00140

Author Contributions

‖A.F. and A.S. contributed equally to this work.

Notes

The authors declare no competing financial interest.

ACKNOWLEDGMENTS

This study was supported by project grant nos. 148556 and 156138 from the Canadian Institutes of Health Research to J.G. and a graduate award from the Centre for Pharmaceutical Oncology to A.F.

REFERENCES

(1) Anselmo, A. C.; Mitragotri, S. Nanoparticles in the Clinic: An Update. *Bioeng. Transl. Med.* **2019**, *4* (3), No. e10143.

(2) Mitchell, M. J.; Billingsley, M. M.; Haley, R. M.; Wechsler, M. E.; Peppas, N. A.; Langer, R. Engineering Precision Nanoparticles for Drug Delivery. *Nat. Rev. Drug Discovery* **2021**, *20* (2), 101−124.

(3) Iijima, M.; Araki, K.; Liu, Q.; Somiya, M.; Kuroda, S. Oriented Immobilization to Nanoparticles Enhanced the Therapeutic Efficacy of Antibody Drugs. *Acta Biomater.* **2019**, *86*, 373−380.

(4) Fornt-Suñé, M.; Bermejo, G. L.; Gil-Garcia, M.; Aran, A.; Garcia-Pardo, J.; Martí, M.; Ventura, S. Protein-Only Nanoparticles for T Cell Expansion and Activation. *ACS Appl. Nano Mater.* **2024**, *7*, 6669−6680.

(5) Gil-Garcia, M.; Ventura, S. Multifunctional Antibody-Conjugated Coiled-Coil Protein Nanoparticles for Selective Cell Targeting. *Acta Biomater.* **2021**, *131*, 472−482.

(6) Begent, R. H. J.; Verhaar, M. J.; Chester, K. A.; Casey, J. L.; Green, A. J.; Napier, M. P.; Hope-Stone, L. D.; Cushen, N.; Keep, P. A.; Johnson, C. J.; Hawkins, R. E.; Hilson, A. J. W.; Robson, L. Clinical Evidence of Efficient Tumor Targetting Based on Single-Chain Fv Antibody Selected from a Combinatorial Library. *Nat. Med.* **1996**, *2* (9), 979−984.

(7) Nilsson, B.; Moks, T.; Jansson, B.; Abrahmsén, L.; Elmblad, A.; Holmgren, E.; Henrichson, C.; Jones, T. A.; Uhlén, M. A Synthetic IgG-Binding Domain Based on Staphylococcal Protein A. *Protein Eng.* **1987**, *1* (2), 107−113.

(8) Walsby, A. E. Gas Vesicles. *Microbiol. Rev.* **1994**, *58* (1), 94−144.

(9) Fernando, A.; Gariépy, J. Coupling Chlorin E6 to the Surface of Nanoscale Gas Vesicles Strongly Enhances Their Intracellular Delivery and Photodynamic Killing of Cancer Cells. *Sci. Rep.* **2020**, *10* (1), 2802.

(10) DasSarma, P.; Negi, V. D.; Balakrishnan, A.; Kim, J.-M.; Karan, R.; Chakravortty, D.; DasSarma, S. Haloarchaeal Gas Vesicle Nanoparticles Displaying Salmonella Antigens as a Novel Approach to Vaccine Development. *Procedia Vaccinol.* **2015**, *9*, 16−23.

(11) Song, L.; Wang, G.; Hou, X.; Kala, S.; Qiu, Z.; Wong, K. F.; Cao, F.; Sun, L. Biogenic Nanobubbles for Effective Oxygen Delivery and Enhanced Photodynamic Therapy of Cancer. *Acta Biomater.* **2020**, *108*, 313−325.

(12) Graff, C. P.; Chester, K.; Begent, R.; Wittrup, K. D. Directed evolution of an anti-carcinoembryonic antigen scFv with a 4-day monovalent dissociation half-time at 37 C. *Protein Eng., Des. Sel.* **2004**, *17* (4), 293−304.

(13) Mackness, B. C.; Jaworski, J. A.; Boudanova, E.; Park, A.; Valente, D.; Mauriac, C.; Pasquier, O.; Schmidt, T.; Kabiri, M.; Kandira, A.; Radošević, K.; Qiu, H. Antibody Fc Engineering for Enhanced Neonatal Fc Receptor Binding and Prolonged Circulation Half-Life. *mAbs* **2019**, *11* (7), 1276−1288.

(14) Butterfield, J. T.; Kim, H.; Knauer, D. J.; Nevala, W. K.; Markovic, S. N. Identification of a Peptide-Peptide Binding Motif in the Coating of Nab-Paclitaxel Nanoparticles with Clinical Antibodies: Bevacizumab, Rituximab, and Trastuzumab. *Sci. Rep.* **2017**, *7* (1), 14476.

(15) Holliger, P.; Manzke, O.; Span, M.; Hawkins, R.; Fleischmann, B.; Qinghua, L.; Wolf, J.; Diehl, V.; Cochet, O.; Winter, G.; Bohlen, H. Carcinoembryonic Antigen (CEA)-Specific T-Cell Activation in Colon Carcinoma Induced by Anti-CD3 × Anti-CEA Bispecific Diabodies and B7 × Anti-CEA Bispecific Fusion Proteins. *Cancer Res.* **1999**, *59* (12), 2909.

(16) Francis, R. J.; Mather, S. J.; Chester, K.; Sharma, S. K.; Bhatia, J.; Pedley, R. B.; Waibel, R.; Green, A. J.; Begent, R. H. J. Radiolabelling of Glycosylated MFE-23::CPG2 Fusion Protein (MFECP1) with 99mTc for Quantitation of Tumour Antibody-Enzyme Localisation in Antibody-Directed Enzyme pro-Drug Therapy (ADEPT). *Eur. J. Nucl. Med. Mol. Imaging* **2004**, *31* (8), 1090−1096.

(17) Fernando, A. Exploring the Theranostic Potential of Gas Vesicle Protein Nanobubbles | TSpace Repository. https://tspace.library.utoronto.ca/handle/1807/108801 (accessed 2024-05-08).

(18) Blumenthal, R. D.; Leon, E.; Hansen, H. J.; Goldenberg, D. M. Expression Patterns of CEACAM5 and CEACAM6 in Primary and Metastatic Cancers. *BMC Cancer* **2007**, *7* (1), 2.

(19) Strunk, T.; Hamacher, K.; Hoffgaard, F.; Engelhardt, H.; Zillig, M. D.; Faist, K.; Wenzel, W.; Pfeifer, F. Structural Model of the Gas Vesicle Protein GvpA and Analysis of GvpA Mutants in Vivo. *Mol. Microbiol.* **2011**, *81* (1), 56−68.

(20) Ljungberg, U. K.; Jansson, B.; Niss, U.; Nilsson, R.; Sandberg, B. E. B.; Nilsson, B. The Interaction between Different Domains of

Staphylococcal Protein A and Human Polyclonal IgG, IgA, IgM and F(Ab')2: Separation of Affinity from Specificity. *Mol. Immunol.* **1993**, *30* (14), 1279−1285.
(21) Hua, Z.; Jie, L.; Zhu, D. Expression of a Fibrinolytically Active Human Pro-Urokinase Fusion Protein in Escherichia Coli. *Biochem. Mol. Biol. Int.* **1994**, *33* (6), 1215−1220.
(22) Inouye, S.; Sahara-Miura, Y. A Fusion Protein of the Synthetic IgG-Binding Domain and Aequorin: Expression and Purification from E. Coli Cells and Its Application. *Protein Expression Purif.* **2017**, *137*, 58−63.
(23) Chen, C.; Huang, Q.-L.; Jiang, S.-H.; Pan, X.; Hua, Z.-C. Immobilized Protein ZZ, an Affinity Tool for Immunoglobulin Isolation and Immunological Experimentation. *Biotechnol. Appl. Biochem.* **2006**, *45* (2), 87−92.
(24) Bhatia, J.; Sharma, S. K.; Chester, K. A.; Pedley, R. B.; Boden, R. W.; Read, D. A.; Boxer, G. M.; Michael, N. P.; Begent, R. H. J. Catalytic Activity Of An In Vivo Tumor Targeted Anti-Cea Scfv::Carboxypeptidase G2 Fusion Protein. *Int. J. Cancer* **2000**, *85*, 571−577.
(25) Kousparou, C. A.; Epenetos, A. A.; Deonarain, M. P. Antibody-Guided Enzyme Therapy of Cancer Producing Cyanide Results in Necrosis of Targeted Cells. *Int. J. Cancer* **2002**, *99* (1), 138−148.
(26) Kimura, H.; Sawada, T.; Oshima, S.; Kozawa, K.; Ishioka, T.; Kato, M. Toxicity and Roles of Reactive Oxygen Species. *Curr. Drug Targets: Inflammation Allergy* **2005**, *4* (4), 489−495.
(27) Kostenich, G. A.; Zhuravkin, I. N.; Furmanchuk, A. V.; Zhavrid, E. A. Photodynamic Therapy with Chlorin E6. A Morphologic Study of Tumor Damage Efficiency in Experiment. *J. Photochem. Photobiol., B* **1991**, *11* (3−4), 307−318.
(28) Nyman, E. S.; Hynninen, P. H. Research Advances in the Use of Tetrapyrrolic Photosensitizers for Photodynamic Therapy. *J. Photochem. Photobiol., B* **2004**, *73* (1−2), 1−28.
(29) Spikes, J. D.; Bommer, J. C. Photosensitizing Properties of Mono-l-Aspartyl Chlorin E6 (NPe6): A Candidate Sensitizer for the Photodynamic Therapy of Tumors. *J. Photochem. Photobiol., B* **1993**, *17* (2), 135−143.
(30) Komolibus, K.; Fisher, C.; Swartling, J.; Svanberg, S.; Svanberg, K.; Andersson-Engels, S. Perspectives on Interstitial Photodynamic Therapy for Malignant Tumors. *J. Biomed. Opt.* **2021**, *26* (07), 070604.
(31) Padalkar, M. V.; Pleshko, N. Wavelength-Dependent Penetration Depth of Near Infrared Radiation into Cartilage. *Analyst* **2015**, *140* (7), 2093−2100.
(32) Chen, Q.; Wang, C.; Cheng, L.; He, W.; Cheng, Z.; Liu, Z. Protein Modified Upconversion Nanoparticles for Imaging-Guided Combined Photothermal and Photodynamic Therapy. *Biomaterials* **2014**, *35* (9), 2915−2923.
(33) Namiot, E. D.; Sokolov, A. V.; Chubarev, V. N.; Tarasov, V. V.; Schiöth, H. B. Nanoparticles in Clinical Trials: Analysis of Clinical Trials, FDA Approvals and Use for COVID-19 Vaccines. *Int. J. Mol. Sci.* **2023**, *24*, 787.
(34) Espelin, C. W.; Leonard, S. C.; Geretti, E.; Wickham, T. J.; Hendriks, B. S. Dual HER2 Targeting with Trastuzumab and Liposomal-Encapsulated Doxorubicin (MM-302) Demonstrates Synergistic Antitumor Activity in Breast and Gastric Cancer. *Cancer Res.* **2016**, *76* (6), 1517−1527.
(35) Study Details|MM-302 Plus Trastuzumab vs. Chemotherapy of Physician's Choice Plus Trastuzumab in HER2-Positive Locally Advanced/Metastatic Breast Cancer Patients|ClinicalTrials.gov. https://clinicaltrials.gov/study/NCT02213744 (accessed 2023-10-17).
(36) Chen, B. M.; Su, Y. C.; Chang, C. J.; Burnouf, P. A.; Chuang, K. H.; Chen, C. H.; Cheng, T. L.; Chen, Y. T.; Wu, J. Y.; Roffler, S. R. Measurement of Pre-Existing IgG and IgM Antibodies against Polyethylene Glycol in Healthy Individuals. *Anal. Chem.* **2016**, *88* (21), 10661−10666.
(37) Roffler, S.; Cheng, T.-L.; Kao, C.-H.; Chen, B.-M.; Su, Y.-C.; Tung, H.-Y.; Chuang, K.-H.. Bi-Specific Antibodies and Uses Thereof. U.S. Patent 11,040,111 B2, June 22, 2021.
(38) Chardès, T.; Villard, S.; Ferrières, G.; Piechaczyk, M.; Cerutti, M.; Devauchelle, G.; Pau, B. Efficient Amplification and Direct Sequencing of Mouse Variable Regions from Any Immunoglobulin Gene Family. *FEBS Lett.* **1999**, *452* (3), 386−394.
(39) Lefranc, M. P.; Pommié, C.; Ruiz, M.; Giudicelli, V.; Foulquier, E.; Truong, L.; Thouvenin-Contet, V.; Lefranc, G. IMGT Unique Numbering for Immunoglobulin and T Cell Receptor Variable Domains and Ig Superfamily V-like Domains. *Dev. Comp. Immunol.* **2003**, *27* (1), 55−77.
(40) Ye, J.; Ma, N.; Madden, T. L.; Ostell, J. M. IgBLAST: An Immunoglobulin Variable Domain Sequence Analysis Tool. *Nucleic Acids Res.* **2013**, *41* (W1), W34−W40.
(41) Sievers, F.; Wilm, A.; Dineen, D.; Gibson, T. J.; Karplus, K.; Li, W.; Lopez, R.; McWilliam, H.; Remmert, M.; Söding, J.; Thompson, J. D.; Higgins, D. G. Fast, Scalable Generation of High-Quality Protein Multiple Sequence Alignments Using Clustal Omega. *Mol. Syst. Biol.* **2011**, *7*, 539.
(42) Ma, Y. H. V.; Sparkes, A.; Romão, E.; Saha, S.; Gariépy, J. Agonistic Nanobodies and Antibodies to Human VISTA. *mAbs* **2021**, *13* (1), 2003281.
(43) Chen, X.; Zhong, Z.; Xu, Z.; Chen, L.; Wang, Y. 2',7'-Dichlorodihydrofluorescein as a Fluorescent Probe for Reactive Oxygen Species Measurement: Forty Years of Application and Controversy. *Free Radical Res.* **2010**, *44* (6), 587−604.
(44) Jumper, J.; Evans, R.; Pritzel, A.; Green, T.; Figurnov, M.; Ronneberger, O.; Tunyasuvunakool, K.; Bates, R.; Žídek, A.; Potapenko, A.; Bridgland, A.; Meyer, C.; Kohl, S. A. A.; Ballard, A. J.; Cowie, A.; Romera-Paredes, B.; Nikolov, S.; Jain, R.; Adler, J.; Back, T.; Petersen, S.; Reiman, D.; Clancy, E.; Zielinski, M.; Steinegger, M.; Pacholska, M.; Berghammer, T.; Bodenstein, S.; Silver, D.; Vinyals, O.; Senior, A. W.; Kavukcuoglu, K.; Kohli, P.; Hassabis, D. Highly Accurate Protein Structure Prediction with AlphaFold. *Nature* **2021**, *596* (7873), 583−589.
(45) Boehm, M. K.; Corper, A. L.; Wan, T.; Sohi, M. K.; Sutton, B. J.; Thornton, J. D.; Keep, P. A.; Chester, K. A.; Begent, R. H. J.; Perkins, S. J. Crystal Structure of the Anti-(Carcinoembryonic Antigen) Single-Chain Fv Antibody MFE-23 and a Model for Antigen Binding Based on Intermolecular Contacts. *Biochem. J.* **2000**, *346* (2), 519.
(46) Boehm, M. K.; Perkins, S. J. Structural Models for Carcinoembryonic Antigen and Its Complex with the Single-Chain Fv Antibody Molecule MFE23. *FEBS Lett.* **2000**, *475* (1), 11−16.
(47) Harris, L. J.; Skaletsky, E.; McPherson, A. Crystallographic structure of an intact IgG1 monoclonal antibody 1 1Edited by I. A. Wilson. *J. Mol. Biol.* **1998**, *275* (5), 861−872.
(48) Ultsch, M.; Braisted, A.; Maun, H. R.; Eigenbrot, C. 3−2-1: Structural Insights from Stepwise Shrinkage of a Three-Helix Fc-Binding Domain to a Single Helix. *Protein Eng., Des. Sel.* **2017**, *30* (9), 619−625.

https://doi.org/10.1021/acsptsci.4c00140
ACS Pharmacol. Transl. Sci. 2024, 7, 1864−1873